J. Fluid Mech. (2004), *vol.* 498, *pp.* 289–313. © 2004 Cambridge University Press
DOI: 10.1017/S0022112003006815 Printed in the United Kingdom

Internal wave fields and drag generated by a translating body in a stratified fluid

By M. M. SCASE AND S. B. DALZIEL

Department of Applied Mathematics and Theoretical Physics, University of Cambridge, Centre for Mathematical Sciences, Wilberforce Road, Cambridge CB3 OWA, UK

(Received 18 December 2002 and in revised form 1 September 2003)

Asymptotic approximations to the velocity and pressure fields generated by steadily towing a body through a uniformly stratified fluid in an arbitrary direction are calculated. This is done explicitly for point sources, both oscillatory and non-oscillatory in strength, and for a spherical source of non-oscillatory strength. The flow fields are divided into regions by causality and radiation conditions which have contributions containing up to three significant internal waves in the non-oscillatory cases, and up to six in the oscillatory cases. A method for describing the caustics is given. The drag due to the internal wave field induced by towing a body through the fluid is calculated for a spherical source, of non-oscillatory strength, being towed at a general tow angle and Froude number. Dependence of the drag coefficient on the tow angle and the Froude number is shown in particular the tow angle can significantly affect the magnitude of the drag coefficient for a given Froude number.

1. Introduction

The importance of internal gravity waves in geophysical flows is well known and has been the subject of many studies. Examples include 'lee waves' produced by a steady wind flowing over a mountain (Lighthill 1978), and the internal waves generated by a slender translating and oscillating body (Rehm & Radt 1975). Internal waves differ dynamically from surface waves in many ways. For example, in internal waves the group and phase velocities are perpendicular, so that energy is transported parallel to the wave crests; in contrast for surface waves the group and phase velocities are parallel and energy propagates normal to the wave crests. Previous research motivated by oceanographic or naval applications has mostly considered internal waves generated by horizontally towed bodies (e.g. Miles 1971; Rehm & Radt 1975; Dupont & Voisin 1996). Other studies have considered the wave fields generated by vertical translation of a body (Warren 1960; Lighthill 1967), which is of interest when trying to understand the rising of thermals through stably stratified regions of the atmosphere. Internal waves generated by a point source being towed in an arbitrary direction in two dimensions have also been examined in detail, for example by Rarity (1967), Stevenson (1968) and, including oscillations of the source, in Stevenson & Thomas (1969). Peat & Stevenson (1975) consider constant phase surfaces of internal waves generated by oscillating point and line sources moving in arbitrary directions in a slightly compressible fluid both theoretically and experimentally. Smirnov & Chashechkin (1998) consider the vertical displacement field for a non-oscillating sphere travelling in an arbitrary direction both theoretically and experimentally.

https://doi.org/10.1017/S0022112003006815 Published online by Cambridge University Press

A new approach to describing internal waves generated by oscillating point sources, cylinders and spheres was adopted by Voisin (1991), which uses Green's functions as opposed to the Fourier-transform-based approach adopted by Lighthill (1960, 1965, 1967). Voisin's approach allows investigation of the waves in real (physical) time and space, and is based upon the wave fields being built up as a superposition of elementary impulses each of which is represented by the Green's function. This approach was later extended to internal waves generated by arbitrarily moving oscillating or non-oscillating point sources in Voisin (1994), where the solutions for horizontal and vertical translation were given explicitly. In Dupont & Voisin (1996) this work was extended further and the wave field generated by a sphere oscillating vertically while steadily translating horizontally was calculated. This theory was shown to agree well with their experimental results.

In a stratified fluid, internal waves propagate away from the source, transporting momentum to other parts of the fluid. This momentum flux is felt by the source as an extra drag, sometimes referred to as 'wave resistance' (e.g. Warren 1960). In Gorodtsov & Teodorovich (1980) it was shown that the expression for the drag due to the waves generated by a point source does not converge. This is because the energy losses are proportional to the pressure at the location of the source, which is infinite. However, Gorodtsov & Teodorovich (1982) calculated the expression for the drag due to waves produced by the horizontal motion of a spherical source, which does converge. The results given by Gorodtsov & Teodorovich (1982) were compared to experimental data by Lofquist & Purtell (1984) in Greenslade (2000), and agreed well for Froude numbers greater than 1. It should be noted that the theory used in Gorodtsov & Teodorovich (1982) is linear and breaks down for Froude numbers less than 1, i.e. very strong stratifications. It was also shown (Lofquist & Purtell 1984) that for sufficiently large Reynolds number ($Re \gtrsim 150$) the wave resistance is almost independent of the Reynolds number.

The drag and lift due to an arbitrarily moving thin disk was given in MacKinnon, Mulley & Warren (1969), where it was shown that the drag coefficient depends on both the Froude number and the angle of attack of the disk. The method in MacKinnon *et al.* (1969) relied on the body being slender. Warren (1960) calculated the wave resistance on a vertically translating slender spindle and a sphere. It was concluded that wave resistance was negligible for a rising thermal, but that it may have a very significant effect on turbulent eddies.

It is of interest to see whether the drag induced by the wave field is significantly affected by the tow angle; this has many applications, but was motivated, in this case, by a study of the effects of stratification on coherent structures in turbulent flows. For example, vortex rings propagate with an approximate free-slip boundary condition through fluid, and so the wave drag cannot be considered negligible compared to the friction drag. Hence it is of interest to see how the wave drag depends on the Froude number and the angle of propagation.

In § 2 a brief summary of the essential results from Voisin (1994) is given. Then in § 3 a method for explicitly calculating the velocity, $\boldsymbol{u}(\boldsymbol{r}, t)$, and pressure perturbation, $P(\boldsymbol{r}, t)$, fields is given for both a non-oscillating and an oscillating point source being towed in an arbitrary direction. It is shown that these fields can be described asymptotically in terms of a vector $\boldsymbol{R}$. The explicit relation given for finding $\boldsymbol{R}$ due to an arbitrary direction of body translation is an extension of the theory given in Voisin (1994). It is also shown in § 3 how the flow field is divided up into distinct regions by wavefronts, and a method for finding these surfaces is given. These results are then extended to give expressions for $\boldsymbol{u}(\boldsymbol{r}, t)$ and $P(\boldsymbol{r}, t)$ for a non-oscillating

https://doi.org/10.1017/S0022112003006815 Published online by Cambridge University Press

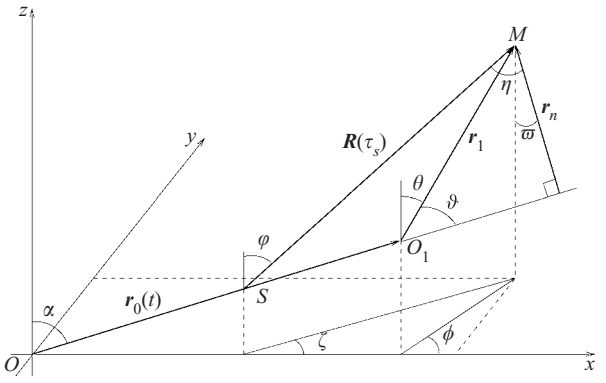


FIGURE 1. The generalized geometrical set up of a wave generated at time τ emitted at the wave source S reaching an arbitrary point M at time t.

spherical source being towed in an arbitrary direction. In §4 the wave drag on a sphere is calculated for both an arbitrary direction of tow and Froude number. The tow angle which gives least resistance, and how the tow angle varies with the Froude number are also considered.

Throughout this paper it will be assumed that the fluid is inviscid, unbounded and has a uniform stratification $\rho_0(z) = \rho_{00} \exp\{-\beta z\}$, where $\beta g = N^2$. Here, N is the buoyancy frequency and is constant, g is the acceleration due to gravity, ρ_{00} is a reference density and $\rho_0(z)$ is the background, hydrostatic density field. The Boussinesq approximation is made whereby density differences in the inertial term of the Euler equation are ignored. It will be assumed that the waves generated are linear and of small amplitude. Finally, attention will be restricted to the case of a body being towed steadily with constant velocity $\boldsymbol{v}_0$ and, without loss of generality, the coordinate system will be chosen so that the motion is symmetric about the $y = 0$ plane.

2. Summary of the Green's function approach

This section reviews the Green's function approach of Voisin (1994) for point sources. Then a method for developing this approach to include extended sources is explained.

2.1. *Point sources*

Consider the generalized coordinate system shown in figure 1. This is the geometrical set up for a wave emitted at the wave source S reaching an arbitrary point M, where S has position vector $\boldsymbol{r}_0(\tau)$ and M has position vector $\boldsymbol{r} = \boldsymbol{r}_0(t) + \boldsymbol{r}_1$. A moving set of coordinates with origin O_1, coincident with the steadily propagating source, moves within a fixed reference frame with origin O. The velocity $\boldsymbol{u}(\boldsymbol{r}, t)$ and pressure perturbation $P(\boldsymbol{r}, t)$ fields can be written in terms of an internal potential $\psi(\boldsymbol{r}, t)$ as (Gorodtsov & Teodorovich 1980; Hart 1981)

$$\boldsymbol{u}(\boldsymbol{r}, t) = \left(\frac{\partial^2}{\partial t^2}\nabla + N^2\nabla_h\right)\psi(\boldsymbol{r}, t), \qquad P(\boldsymbol{r}, t) = -\rho_0\left(\frac{\partial^2}{\partial t^2} + N^2\right)\frac{\partial}{\partial t}\psi(\boldsymbol{r}, t), \quad (2.1)$$

https://doi.org/10.1017/S0022112003006815 Published online by Cambridge University Press

where $\nabla_h = (\partial_x, \partial_y, 0)$, and the internal potential satisfies the continuity equation

$$\nabla \cdot \boldsymbol{u} \equiv \left(\frac{\partial^2}{\partial t^2} \nabla^2 + N^2 \nabla_h^2 \right) \psi(\boldsymbol{r}, t) = m(\boldsymbol{r} - \boldsymbol{r}_0(t), t), \tag{2.2}$$

where m is the source term and P is the perturbation to the hydrostatic pressure field. Equations (2.1) and (2.2) come from linearizing the Euler equations under the assumption that the fluid velocities, $\boldsymbol{u}(\boldsymbol{r}, t)$, and the pressure perturbation, $P(\boldsymbol{r}, t)$, are small compared to the tow speed, v_0, and the hydrostatic pressure respectively.

In general, for a time τ such that $0 \leqslant \tau \leqslant t$ a point source of the form

$$m(\boldsymbol{r}, t) = m_0 \mathrm{e}^{\mathrm{i}\omega_0 t} \delta(\boldsymbol{r}) \tag{2.3}$$

will be considered, where δ is the Dirac delta function and ω_0 is the frequency of oscillation of the source's strength. The vector $\boldsymbol{R}(\tau)$ denotes the vector from the general path point $\boldsymbol{r}_0(\tau)$ (i.e. the position of O_1 at $t = \tau$) to the general point M. In the special case of a non-oscillating source, $\omega_0 = 0$, the asymptotic expression for the internal potential, valid for $(t - \tau)N \gg 1$, is

$$\psi(\boldsymbol{r}, t) \sim -\frac{1}{(2\pi)^{3/2} N} \int_0^t \frac{m_0}{R_h(\tau)} \left\{ \frac{\cos\left[(t-\tau)N|R_z(\tau)|/R(\tau) - \frac{1}{4}\pi\right]}{[(t-\tau)N|R_z(\tau)|/R(\tau)]^{1/2}} + \frac{\sin\left[(t-\tau)N - \frac{1}{4}\pi\right]}{[(t-\tau)N]^{1/2}} \right\} \mathrm{d}\tau, \tag{2.4}$$

where $\boldsymbol{R} = (R_x, R_y, R_z)$, $\boldsymbol{R}_h = (R_x, R_y, 0)$, $R = |\boldsymbol{R}|$ and $R_h = |\boldsymbol{R}_h|$. The cosine term represents gravity waves of frequency $\omega = R_z(\tau)N/R(\tau)$ propagating at an angle φ to the vertical where $\cos\varphi = R_z(\tau)/R(\tau)$. The sine term represents buoyancy oscillations with frequency N. Due to their amplitude, buoyancy oscillations are negligible compared to gravity waves built up by the motion of the source, and so accordingly the phase, $\Phi(\tau)$, is defined as

$$\Phi(\tau) = (t - \tau)N \frac{|R_z(\tau)|}{R(\tau)}. \tag{2.5}$$

If the body is impulsively started from rest, a spectrum of waves is generated of all frequencies. These waves are referred to as transient waves in Voisin (1994). Within regions where waves are built up due to the translation of the source the waves are referred to as permanent waves, and within these regions transient waves are negligible. On the boundary of the region between permanent waves and transient waves, the wave crests always merge. Since the contribution to the wave drag from these transient waves is negligible and they are negligible within the region containing permanent waves, these transient waves will henceforth be ignored.

The retarded time, τ_s, is the time when the most significant wave contributions to the wave field at M were emitted (see figure 1), i.e. the most significant contribution to the wave field at M was generated by the source at $t = \tau_s$ and has reached the point M at time t. The method of stationary phase gives a retarded time τ_s, where $\partial\Phi(\tau)/\partial\tau|_{\tau=\tau_s} = 0$. This is because in the neighbourhood of $\tau = \tau_s$, Φ varies slowly and there is little cancellation of contributions to ψ due to oscillations from the

https://doi.org/10.1017/S0022112003006815 Published online by Cambridge University Press

cosine term in (2.4). Applying this technique to (2.5) gives the retarded time equation

$$t - \tau_s = \frac{R(\tau_s)}{\boldsymbol{v}_0 \cdot \left[\dfrac{\boldsymbol{R}(\tau_s)}{R(\tau_s)} - \dfrac{R(\tau_s)}{R_z(\tau_s)}\boldsymbol{e}_z\right]}, \tag{2.6}$$

where $\boldsymbol{e}_z$ is a unit vector pointing in the vertical, z, direction.

The internal potential field can be asymptotically described in terms of $\boldsymbol{R}(\tau_s)$, and is a Liénard–Wiechert potential (Reitz & Milford 1960) for internal waves. For the source given in (2.3), $\psi(\boldsymbol{r}, t)$ is equal to the real part of $m_0\Psi(\boldsymbol{r}, t)$, i.e.

$$\psi(\boldsymbol{r}, t) \sim \mathrm{Re}[m_0\Psi(\boldsymbol{r}, t)], \tag{2.7}$$

where Re denotes the real part,

$$\Psi(\boldsymbol{r}, t) \sim -\frac{1}{2\pi N^2|A|^{1/2}} \frac{R(\tau_s)}{R_h(\tau_s)|R_z(\tau_s)|} \exp\left\{\mathrm{i}\left[\frac{N}{c_g}|R_z(\tau_s)| - \frac{\pi}{2}H(-A)\right]\right\}, \tag{2.8}$$

and H is the Heaviside function. In (2.8), c_g is the modulus of the group velocity, $\boldsymbol{c}_g$, the velocity with which the wave has travelled from the source S to the general point M, i.e.

$$\boldsymbol{c}_g(\tau_s) = \frac{\boldsymbol{R}(\tau_s)}{(t - \tau_s)} = \boldsymbol{v}_0 \cdot \left[\frac{\boldsymbol{R}(\tau_s)}{R(\tau_s)} - \frac{R(\tau_s)}{R_z(\tau_s)}\boldsymbol{e}_z\right] \frac{\boldsymbol{R}(\tau_s)}{R(\tau_s)}. \tag{2.9}$$

The quantity A for a non-accelerating, non-oscillating source is

$$A = -\left(\frac{\boldsymbol{v}_0}{c_g} \times \frac{\boldsymbol{R}}{R}\right)^2 + 2\frac{\boldsymbol{v}_0}{c_g} \cdot \frac{R}{R_z}\boldsymbol{e}_z\bigg|_{\tau=\tau_s}. \tag{2.10}$$

This comes from the second derivative of the phase, Φ, with respect to τ in the stationary phase approximation.

The frequency, ω (defined such that $\Phi = (t - \tau)\omega$), and the wavenumber vector, $\boldsymbol{k} = -\nabla\Phi|_{\tau=\tau_s}$, are given by

$$\omega = N\frac{|R_z(\tau_s)|}{R(\tau_s)}, \qquad \boldsymbol{k} = \frac{\omega}{c_g}\left(\frac{\boldsymbol{R}}{R} - \frac{R}{R_z}\boldsymbol{e}_z\right). \tag{2.11}$$

The pressure and velocity fields are given respectively, from (2.1), by

$$P(\boldsymbol{r}, t) \sim \frac{\rho_0 N m_0}{2\pi} \frac{R_h}{R^2} \frac{\cos\left[N|R_z|/c_g + \frac{1}{2}\pi H(A)\right]}{|A|^{1/2}}, \tag{2.12}$$

$$\boldsymbol{u}(\boldsymbol{r}, t) \sim \frac{N m_0}{2\pi c_g} \frac{R_h}{R^2} \frac{\boldsymbol{R}}{R} \frac{\cos\left[N|R_z|/c_g + \frac{1}{2}\pi H(A)\right]}{|A|^{1/2}}. \tag{2.13}$$

Hence a complete asymptotic description of the wave fields generated by a non-oscillating arbitrarily moving point source can be found, once a method for finding the vector $\boldsymbol{R}(\tau_s)$ has been established. If the solution to (2.6) is not unique, so that more than one solution $\boldsymbol{R}(\tau_s)$ exists for a given $\boldsymbol{r}(t)$, then the wave field is the superposition of all such solutions.

If the source is oscillating, i.e. $\omega_0 \neq 0$ in equation (2.3), then the asymptotic expression for the phase is

$$\Phi_{\pm}(\tau) = \tau\omega_0 \pm (t - \tau)N\frac{|R_z|}{R}. \tag{2.14}$$

https://doi.org/10.1017/S0022112003006815 Published online by Cambridge University Press

The two waves represented by the choice of sign can be interpreted as the beating of waves between those generated by the motion of the source and those generated by the oscillation of the source (Voisin 1994). Using (2.14), the stationary phase condition gives the modified retarded time equation (cf. equation (2.6))

$$t-\tau_{s\pm}=\left(1\mp\frac{R(\tau_{s\pm})\omega_0}{N|R_z(\tau_{s\pm})|}\right)\frac{R(\tau_{s\pm})}{\boldsymbol{v}_0\cdot\left(\dfrac{\boldsymbol{R}(\tau_{s\pm})}{R(\tau_{s\pm})}-\dfrac{R(\tau_{s\pm})}{R_z(\tau_{s\pm})}\boldsymbol{e}_z\right)}, \tag{2.15}$$

where the subscript $\pm$ corresponds to the choice of sign in (2.14). The pressure and velocity field are given respectively, again using equation (2.1), by the real part of

$$P(\boldsymbol{r},t)\sim\frac{\rho_0 N m_0}{4\pi}\frac{R_{h\pm}}{R_\pm^2}\frac{\exp\left\{\mathrm{i}\left[\omega_0\tau_{s\pm}\pm N|R_{z\pm}|/c_{g\pm}\pm\frac{1}{2}\pi H(A_\pm)\right]\right\}}{|A_\pm|^{1/2}}, \tag{2.16}$$

$$\boldsymbol{u}(\boldsymbol{r},t)\sim\frac{N m_0}{4\pi c_{g\pm}}\frac{R_{h\pm}}{R_\pm^2}\frac{\boldsymbol{R}_\pm}{R_\pm}\frac{\exp\left\{\mathrm{i}\left[\omega_0\tau_{s\pm}\pm N|R_{z\pm}|/c_{g\pm}\pm\frac{1}{2}\pi H(A_\pm)\right]\right\}}{|A_\pm|^{1/2}}, \tag{2.17}$$

where, for a non-accelerating source,

$$A=-\left(\frac{\boldsymbol{v}_0}{c_{g\pm}}\times\frac{\boldsymbol{R}_\pm}{R_\pm}\right)^2+2\left(1\mp\frac{\omega_0}{N}\frac{R_\pm}{|R_{z\pm}|}\right)\left(\frac{\boldsymbol{v}_0}{c_{g\pm}}\cdot\frac{R_\pm}{R_{z\pm}}\boldsymbol{e}_z\mp\frac{\omega_0}{N}\frac{R_\pm}{|R_{z\pm}|}\right)\Bigg|_{\tau=\tau_s}. \tag{2.18}$$

For the flows under consideration here, the only physically valid waves are those which do not enter the flow region through the boundary (Lighthill 1960). Waves which satisfy this criterion are said to obey the *radiation condition*. Since the dispersion relation for internal waves is $\omega=N\cos\varphi$, where φ is the angle the wave beam makes with the vertical (see figure 1), the waves travel in straight lines, i.e. since N and ω are constant for a given wave, φ is constant. Hence, the radiation condition is equivalent to requiring that for a wave generated at $\boldsymbol{r}_0(\tau_s)$ to reach M, the group velocity, $\boldsymbol{c}_g$, is not only proportional to $\boldsymbol{R}(\tau_s)$, but it also points in the same direction.

One significant advantage of Voisin's Green's function approach over the method adopted by Lighthill (1960, 1965, 1967) is that it shows whether the retarded time, τ_s, obeys the causality condition $0\leqslant\tau_s\leqslant t$, given that the motion of the body was initiated at $t=0$. Causality is the temporal equivalent of the spatial radiation condition, meaning that waves may only be observed after they have been emitted. Voisin's method means that a *causality envelope* can be drawn showing the instantaneous region of fluid in motion due to internal waves generated by previous movement of the source, whereas Lighthill's method assumed that the source had been towed for infinite time.

2.2. *Extended sources*

The generalization of the point source theory presented in the previous sub-section to that of an extended source (e.g. a sphere) has been used previously in Dupont & Voisin (1996). No indication of the derivation was presented however, and so a brief summary is given here.

It follows from (2.4) that the internal potential (ignoring buoyancy oscillations as in section § 2.1) with arbitrary source distribution $m(\boldsymbol{r},t)$ and the large time

https://doi.org/10.1017/S0022112003006815 Published online by Cambridge University Press

approximation, $(t-\tau)N \gg 1$, is

$$\psi(\boldsymbol{r},t) \sim -\frac{1}{(2\pi)^{3/2}N}\int_{\mathbb{R}^3}\int_0^t \frac{m(\boldsymbol{r}',\tau)}{|\boldsymbol{R}_h(\tau)-\boldsymbol{r}'_h|}\frac{\cos\left[(t-\tau)N\dfrac{|R_z(\tau)-r'_z|}{|\boldsymbol{R}(\tau)-\boldsymbol{r}'|}-\frac{1}{4}\pi\right]}{\left[(t-\tau)N\dfrac{|R_z(\tau)-r'_z|}{|\boldsymbol{R}(\tau)-\boldsymbol{r}'|}\right]^{1/2}}\,\mathrm{d}\tau\,\mathrm{d}\boldsymbol{r}'. \tag{2.19}$$

For $R \gg r'$ the phase, Φ, may be written as

$$(t-\tau)N\frac{|R_z(\tau)-r'_z|}{|\boldsymbol{R}(\tau)-\boldsymbol{r}'|} \sim (t-\tau)N\frac{|R_z(\tau)|}{R(\tau)} + \boldsymbol{k}(\tau)\cdot\boldsymbol{r}', \tag{2.20}$$

which follows from the definition of $\boldsymbol{k}$ in (2.11) rewritten as

$$\boldsymbol{k}(\tau) = \frac{(t-\tau)N}{R(\tau)}\frac{\boldsymbol{R}(\tau)}{R(\tau)}\times\left(\frac{\boldsymbol{R}(\tau)}{R(\tau)}\times\boldsymbol{e}_z\right)\mathrm{sgn}[R_z(\tau)]. \tag{2.21}$$

The method of stationary phase is then applied to (2.19), since the amplitude of the integrand varies far slower than the phase. The method of stationary phase shows that for rapidly varying $\Phi(\tau)$ and slowly varying $g(\boldsymbol{r}',\tau)$ then

$$\int_0^t\int_{\mathbb{R}^3} \mathrm{e}^{\mathrm{i}\Phi(\tau)}g(\boldsymbol{r}',\tau)\,\mathrm{d}\boldsymbol{r}'\,\mathrm{d}\tau \sim \exp\left\{\mathrm{i}\left[\Phi(\tau_s)+\tfrac{1}{2}\pi H(\Phi''(\tau_s))-\tfrac{1}{4}\pi\right]\right\} \times\sqrt{\frac{2\pi}{|\Phi''(\tau_s)|}}\int_{\mathbb{R}^3} g(\boldsymbol{r}',\tau_s)\,\mathrm{d}\boldsymbol{r}', \tag{2.22}$$

where τ_s is a solution of $\Phi'(\tau)=0$. (Φ is expanded as a Taylor series in $\tau-\tau_s$ and then the τ integral is evaluated using Fresnel integrals.) Then, to evaluate (2.19), $g(\boldsymbol{r}',\tau)$ is defined such that

$$g(\boldsymbol{r}',\tau) = -\frac{m(\boldsymbol{r}',\tau)}{(2\pi)^{3/2}N}\frac{\exp\left\{\mathrm{i}\left(\boldsymbol{k}\cdot\boldsymbol{r}'-\frac{1}{4}\pi\right)\right\}}{|\boldsymbol{R}_h(\tau)-\boldsymbol{r}'_h|\,[\Phi(\tau)+\boldsymbol{k}\cdot\boldsymbol{r}']^{1/2}}. \tag{2.23}$$

This gives the result that for $R \gg r'$ and $(t-\tau)N \gg 1$, to leading order

$$\int_{\mathbb{R}^3} g(\boldsymbol{r}',\tau_s)\,\mathrm{d}\boldsymbol{r}' \sim -\frac{1}{(2\pi)^{3/2}N}\frac{\mathrm{e}^{-\mathrm{i}\pi/4}}{R_h\sqrt{\Phi(\tau_s)}}\int_{\mathbb{R}^3}\mathrm{e}^{\mathrm{i}\boldsymbol{k}\cdot\boldsymbol{r}'}m(\boldsymbol{r}',\tau_s)\,\mathrm{d}\boldsymbol{r}'. \tag{2.24}$$

The integral in the right-hand side of (2.24) is the spatial Fourier transform of the source distribution $m(\boldsymbol{r},\tau)$ at $\tau=\tau_s$, denoted $M(\boldsymbol{k},\tau_s)$. Thus, for Φ defined as in (2.5), combining (2.19) and (2.22) gives the expression for the internal potential for an extended source as

$$\psi(\boldsymbol{r},t) \sim -\frac{1}{2\pi N^2|A|^{1/2}}\frac{R(\tau_s)}{R_h(\tau_s)|R_z(\tau_s)|}\mathrm{Re}\left\{M(\boldsymbol{k},\tau_s)\exp\left[\mathrm{i}\left(\frac{N}{c_g}|R_z(\tau_s)|-\tfrac{1}{2}\pi H(-A)\right)\right]\right\}. \tag{2.25}$$

This is a generalized version of (2.8), so that $\psi(\boldsymbol{r},t) \sim \mathrm{Re}\,[M(\boldsymbol{k},\tau_s)\Psi(\boldsymbol{r},t)]$, where $\boldsymbol{k}$ is found from (2.11). The quantities A, $\boldsymbol{R}$ and c_g which appear in (2.25) are exactly the same as in section § 2.1. Hence it follows from (2.1) that the velocity and pressure perturbation, in the far field are asymptotically equal to their values for a point source of strength 1, multiplied by the spatial Fourier transform of the extended source evaluated at $\tau=\tau_s$.

https://doi.org/10.1017/S0022112003006815 Published online by Cambridge University Press

3. Internal waves generated by an arbitrarily moving source

The theory presented in Voisin (1994) is completely general, but no explicit method is given for finding $\boldsymbol{R}$ when the tow angle α is general. In fact Voisin treated the vertical and horizontal translating cases separately. The possibility of more than one significant wave contribution to the flow at M at time t is avoided by only considering these two cases. In this section a general method will be given for finding $\boldsymbol{R}$ for any angle of tow.

Without loss of generality, the symmetry and the orientation of the coordinate system means that $0 \leqslant \alpha \leqslant \pi/2$ is the only range of tow angle that needs to be considered. Because the wave fields no longer only consist of only one wave, boundaries between regions containing different numbers of waves are present within the flow. A method for describing these wavefronts is also given in this section.

Flows generated by bodies towed through uniformly stratified fluids are characterized by the Froude number, which can be interpreted as the ratio of inertial forces to buoyancy forces, giving a measure of the effective strength of the stratification. When considering the wave field generated by a sphere (or an arbitrary finite non-degenerate body) the Froude number is defined as $Fr = v_0/Na$, where a is the sphere's radius (or an appropriate length scale in the case of an arbitrary body). However, for a point source, where no such length scale is available, the flow is considered to be the limiting case as $Fr \to \infty$.

3.1. *Non-oscillating point sources*

A method for finding the vector $\boldsymbol{R}(\tau_s)$ is now considered. The position vector of a general point $\boldsymbol{r}_1(t)$ in the moving set of coordinates is described, in spherical polar coordinates, by

$$\boldsymbol{r}_1(t) = r_1(\sin\theta\cos\phi, \sin\theta\sin\phi, \cos\theta), \tag{3.1}$$

where $0 \leqslant \theta < \pi$, and $0 \leqslant \phi < 2\pi$. The source path is given by $\boldsymbol{r}_0(t) = \boldsymbol{v}_0 t$, and the tow angle $0 \leqslant \alpha \leqslant \pi/2$ is defined to be the angle between the tow direction and the vertical (see figure 1). The vector $\boldsymbol{R}(\tau_s)$ can be written in terms of the angles φ and ζ as

$$\boldsymbol{R}(\tau_s) = R(\sin\varphi\cos\zeta, \sin\varphi\sin\zeta, \cos\varphi). \tag{3.2}$$

Initially the source will be taken to be non-oscillating, i.e. with $\omega_0 = 0$ in (2.3). In Voisin (1994) the expression for $\boldsymbol{R}(\tau_s)$ is given explicitly for the vertical case $\alpha = 0$, and horizontal case $\alpha = \pi/2$. The angle η, which lies in the range $-\pi/2 \leqslant \eta \leqslant \pi/2$, is the angle between the vector $\boldsymbol{R}(\tau_s)$ and the vector through M which is normal to the tow line, $\boldsymbol{r}_n$ (see figure 1). In the case where $\boldsymbol{v}_0$ is vertical, the angle η is given by the solution of the cubic (Voisin 1994)

$$\tan^3\eta + 2\tan\eta - \cot\theta = 0. \tag{3.3}$$

Equation (3.3) is derived from the retarded time equation (2.6).

Here, an analogous expression for η is derived for a general tow angle α. Using the retarded time equation (2.6) and the geometrical relationships given in figure 1 (i.e. that the distance from S to O_1 is $(t - \tau_s)v_0$), it can be shown that

$$\left(\sin\eta - \frac{\cos\eta\cos\vartheta}{\sin\vartheta}\right)\left(\sin\eta - \frac{\cos\alpha}{\cos\varphi}\right) - 1 = 0, \tag{3.4}$$

where ϑ is the angle between $\boldsymbol{r}_1$ and $\boldsymbol{r}_0$, with $0 \leqslant \vartheta \leqslant \pi$. (A method for finding the equivalent relation to (3.4) for an oscillating point source is outlined in Appendix A.)

https://doi.org/10.1017/S0022112003006815 Published online by Cambridge University Press

The angle ϑ is found from the scalar product of $\hat{\boldsymbol{r}}_1$ and $\hat{\boldsymbol{r}}_0$, giving

$$\cot\vartheta = \frac{\sin\theta\cos\phi\sin\alpha + \cos\theta\cos\alpha}{\{\sin^2\theta\sin^2\phi + (\cos\theta\sin\alpha - \sin\theta\cos\phi\cos\alpha)^2\}^{1/2}}. \tag{3.5}$$

By defining $\boldsymbol{r}_n = (r_{nx}, r_{ny}, r_{nz}) = \boldsymbol{r}_1 - (\boldsymbol{r}_1\cdot\hat{\boldsymbol{r}}_0)\hat{\boldsymbol{r}}_0$, and the angle ϖ, such that $r_{nz}/r_n = \cos\varpi$ $(-\pi\leqslant\varpi\leqslant\pi)$, equation (3.4) can also be written, analogously to equation (3.3), in terms of known quantities as follows. Using the relation

$$\cos\varphi = \cos\alpha\sin\eta + \cos\varpi\cos\eta, \tag{3.6}$$

which can be derived, using geometrical arguments, from figure 1, (3.4) can be written as a cubic in $\tan\eta$, i.e.

$$\tan^3\eta + \left(\frac{\cos\varpi}{\cos\alpha}\cot\vartheta + 2\right)\tan\eta + \frac{\cos\varpi}{\cos\alpha} - \cot\vartheta = 0, \tag{3.7}$$

and $\cos\varpi$ can also be written in terms of known quantities as

$$\cos\varpi = \frac{(\cos\theta\sin\alpha - \sin\theta\cos\phi\cos\alpha)\sin\alpha}{\{\sin^2\theta\sin^2\phi + (\cos\theta\sin\alpha - \sin\theta\cos\phi\cos\alpha)^2\}^{1/2}}. \tag{3.8}$$

The quantities $\hat{\boldsymbol{r}}_0$, $\hat{\boldsymbol{r}}_1$ and $\hat{\boldsymbol{r}}_n$ denote unit vectors in the direction of $\boldsymbol{r}_0$, $\boldsymbol{r}_1$ and $\boldsymbol{r}_n$ respectively. Note that (3.3) is retrieved when $\alpha = 0$ in (3.7) because $\cos\varpi = 0$ and $\vartheta = \theta$ and when $\alpha = \pi/2$, $\eta = \pi - \vartheta$. Both (3.3) and (3.7) are of the same form, i.e. they do not have a quadratic term in $\tan\eta$. Once the angle η is known, the angles φ and ζ required to calculate $\boldsymbol{R}(\tau_s)$ (see equation (3.2)) can be found. First, φ is found from (3.6) then ζ is obtained by simultaneously solving

$$\left.\begin{aligned}[\boldsymbol{R}(\tau_s) - \boldsymbol{r}_1(t)]\cdot\boldsymbol{e}_y = 0,\\ [\boldsymbol{R}(\tau_s) - \boldsymbol{r}_1(t)]\cdot\boldsymbol{r}_n = 0,\end{aligned}\right\} \tag{3.9}$$

where $\boldsymbol{e}_y$ is a unit vector pointing in the y-direction. The relations given in (3.9) arise because $\boldsymbol{R}(\tau_s) - \boldsymbol{r}(t)$ is proportional to $\boldsymbol{r}_0$ which is by definition perpendicular to both $\boldsymbol{e}_y$ and $\boldsymbol{r}_n$. This means that the vector $\boldsymbol{R}(\tau_s)$ can now be found and is given by

$$\boldsymbol{R}(\tau_s) = r_1\begin{pmatrix}\sin\theta\cos\phi\cos^2\alpha + \sin\alpha\sin\vartheta\tan\eta - \sin\alpha\cos\alpha\cos\theta\\ \sin\theta\sin\phi\\ \cos\theta\sin^2\alpha + \cos\alpha\sin\vartheta\tan\eta - \sin\alpha\cos\alpha\sin\theta\cos\phi\end{pmatrix}. \tag{3.10}$$

Hence, calculating the internal wave field in practice amounts to first finding the angles ϑ and ϖ from (3.5) and (3.8) given a position $\boldsymbol{r}_1$ as in (3.1). The angle η is then obtained by solving (3.7). The vector $R(\tau_s)$ is then calculated from (3.10). Once this vector is known, the waves are given by (2.10) and (2.12)–(2.13) for a non-oscillating source, (2.16)–(2.18) for an oscillating source and (2.25) for a non-oscillating extended source. Voisin's results for horizontal towing of a point source are recovered in the limit $\alpha\to\pi/2$ since $\tan\vartheta = \{\sin^2\theta\sin^2\phi + \cos^2\theta\}^{1/2}/\sin\theta\cos\phi$.

Using the relations given in § 2, these results now completely describe the internal waves generated by a non-oscillating point source towed steadily at an arbitrary angle. In particular

$$\Phi = \frac{r_1 N}{v_0}\frac{\sin\vartheta}{\cos\eta}\frac{(\tan\eta\cos\alpha + \cos\varpi)^2}{\tan\eta\cos\varpi - \cos\alpha}\mathrm{sgn}(\cos\alpha\tan\eta + \cos\varpi), \tag{3.11}$$

$$t - \tau_s = \frac{r_1\sin\vartheta}{v_0\cos^2\eta}\left(\frac{\cos\alpha\tan\eta + \cos\varpi}{\cos\varpi\tan\eta - \cos\alpha}\right), \tag{3.12}$$

https://doi.org/10.1017/S0022112003006815 Published online by Cambridge University Press

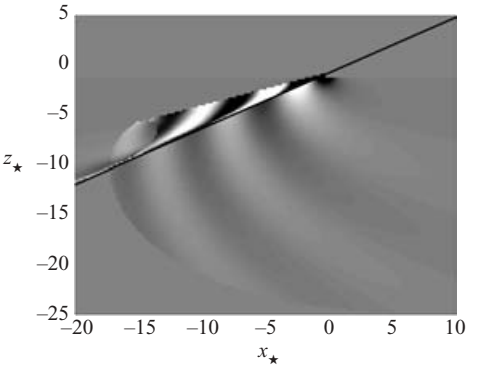


FIGURE 2. The vertical velocity field for a point source which has been towed at an angle $\alpha = \pi/3$, for $t_\star = 20$. The axes have been non-dimensionalized with $x_\star = xN/v_0$, $z_\star = zN/v_0$, $y_\star = yN/v_0 = 0$ and $t_\star = tN$. The dark black line is the tow line.

and

$$\boldsymbol{c}_g(\tau_s) = \frac{v_0 \cos^2\eta}{r_1 \sin\vartheta}\left(\frac{\cos\varpi\tan\eta - \cos\alpha}{\cos\alpha\tan\eta + \cos\varpi}\right)\boldsymbol{R}(\tau_s), \tag{3.13}$$

and in the limit $t \to \infty$, this agrees with Lighthill's Fourier-transform-based approach (Lighthill 1960, 1965, 1967, 1978). For the vertical and horizontal cases considered by Voisin (1994), there is only one real solution of (3.7) for $\tan\eta$. This is not true for a general tow angle. Since equation (3.7) is a cubic, it is possible that there are three real solutions for $\tan\eta$, and hence three corresponding vectors $\boldsymbol{R}(\tau_s)$, although not all solutions will necessarily satisfy both the causality and radiation conditions. The asymptotic expressions (2.12) and (2.13) give the pressure and velocity fields respectively when summed over all valid solutions $\boldsymbol{R}(\tau_s)$, by superposition of these linear waves.

The plot in figure 2 shows the vertical component of the velocity field, obtained using this method, for a point source (this plot does not include the transient start-up waves which have been considered to be negligible). The axes have been non-dimensionalized using $x_\star = xN/v_0$, $y_\star = yN/v_0$ and $z_\star = zN/v_0$ and the angle of tow is $\alpha = \pi/3$. In figure 2 the point has been towed, in the $y_\star = 0$ plane, for $t_\star = 20$, where $t_\star$ is the non-dimensional time given by $t_\star = tN$. The grey scaling is arbitrary, but is the same for figures 9 and 11. White represents maximum upward vertical velocity and black represents maximum downward vertical velocity. The light and dark bands beneath the tow line show the 'lines of constant phase' referred to by Rarity (1967), Stevenson (1968) and many others.

3.2. *Wave analysis*

This sub-section presents a detailed description of the generated waves, analogously to those presented by Rarity (1967) and Stevenson (1968). Indeed, it can be shown that the two-dimensional internal waves generated by an arbitrarily moving source (as in Rarity 1967 and Stevenson 1968) are identical to those in the $y = 0$ plane generated by an arbitrarily moving point source (as in the present paper), apart from their amplitude.

Rarity (1967) identifies the points where lines of constant phase touch the line of tow and where they cross the plane dividing the upstream flow from the downstream flow. Also identified are the series of cusped waves which touch the caustics trailing behind the line of tow. The corresponding wave features are discussed in the present

https://doi.org/10.1017/S0022112003006815 Published online by Cambridge University Press

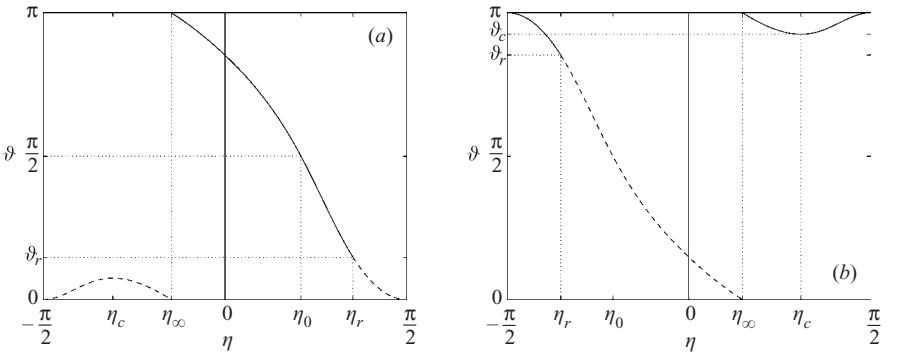


FIGURE 3. The dependence of ϑ on η for (*a*) $\Lambda < 0$ and (*b*) $\Lambda > 0$ ($\Lambda = -2$ and $\Lambda = 2$ respectively). Solid lines represent solutions to (3.14) where the waves satisfy the radiation condition and dashed lines represent solutions to (3.14) where the waves do not satisfy the radiation condition.

paper. (Stevenson (1968) showed that these theoretical predictions agreed well with experimental evidence.)

Defining $\Lambda = \cos\varpi / \cos\alpha$, equation (3.7) can be rewritten† as

$$\cot\vartheta = \frac{\tan^3\eta + 2\tan\eta + \Lambda}{1 - \Lambda\tan\eta}. \tag{3.14}$$

In figure 3 the dependence of ϑ on η is shown for the two cases $\Lambda < 0$ and $\Lambda > 0$. The behaviour of ϑ depends on the four values of η, namely η_c, η_∞, η_0 and η_r, shown in figure 3. The value η_0 is chosen such that $\cot\vartheta_0 = 0$, hence

$$\eta_0 = \tan^{-1}\left\{\left[\left(\frac{\Lambda^2}{4} + \frac{8}{27}\right)^{1/2} - \frac{\Lambda}{2}\right]^{1/3} - \left[\left(\frac{\Lambda^2}{4} + \frac{8}{27}\right)^{1/2} + \frac{\Lambda}{2}\right]^{1/3}\right\}, \tag{3.15}$$

with the corresponding value $\vartheta_0 = \pi/2$. The $\vartheta = \vartheta_0$ plane corresponds to the plane which passes through O_1 with $\boldsymbol{r}\cdot\boldsymbol{r}_0 = 0$ and therefore separates the upstream waves from the downstream waves; η_∞ is defined such that as $\eta \to \eta_\infty$ then $|\cot\vartheta| \to \infty$, i.e.

$$\eta_\infty = \cot^{-1}\Lambda, \qquad \vartheta_\infty = \pi. \tag{3.16}$$

This value of $\eta = \eta_\infty$ corresponds to $\boldsymbol{r}_1 \propto \boldsymbol{r}_0$ where the point M (see figure 1) lies on the source path.

It can be seen from figure 3(*b*) that for values of ϑ below ϑ_c there is only one solution η, but above ϑ_c there are three possible values of η. Therefore ϑ_c divides the region where there are three possible values of η from the region where there is only one. Hence $\vartheta = \vartheta_c$ defines a caustic. The corresponding value of $\eta = \eta_c$ is found from the turning point of (3.14) and is given by

$$\eta_c = \tan^{-1}\left\{\frac{1}{\Lambda}\left[\cosh\left(\frac{\cosh^{-1}(1 + 4\Lambda^2 + 2\Lambda^4)}{3}\right) + \frac{1}{2}\right]\right\}, \tag{3.17}$$

and hence

$$\vartheta_c = \frac{\pi}{2} - \tan^{-1}\left(\frac{\tan^3\eta_c + 2\tan\eta_c + \Lambda}{1 - \Lambda\tan\eta_c}\right). \tag{3.18}$$

† Analysis of equation (3.7) in this form was suggested by an anonymous referee.

https://doi.org/10.1017/S0022112003006815 Published online by Cambridge University Press

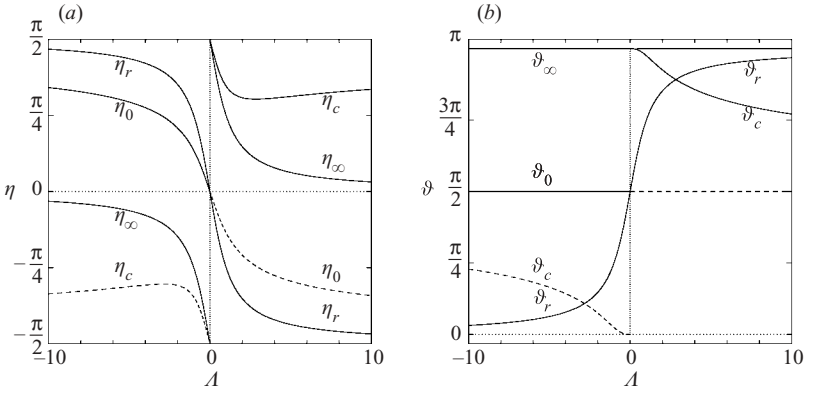


FIGURE 4. Graphs showing the variation of the four values of (*a*) η and (*b*) ϑ defined in (3.16)–(3.19) with the parameter Λ.

The final significant value of η is $\eta = \eta_r$ and corresponds to the point at which $t = \tau_s$ where the waves have just been emitted. Equation (3.12) implies that

$$\eta_r = -\tan^{-1}\Lambda, \qquad \vartheta_r = \frac{\pi}{2} + \tan^{-1}\Lambda, \tag{3.19}$$

and that the causality condition, $t - \tau_s > 0$, is satisfied for waves where $(\tan\eta + \Lambda)(\Lambda\tan\eta - 1) > 0$. For $\Lambda < 0$ this corresponds to values of η such that $\eta_\infty < \eta < \eta_r$ and for $\Lambda > 0$ this corresponds to values of η such that either $\eta < \eta_r$ or $\eta > \eta_\infty$. The behaviour of these four values of η and ϑ with changes in Λ is shown in figure 4.

For all points $\boldsymbol{r}$ above the line of tow, $r_{nz} > 0$, and hence $\Lambda > 0$, and similarly for all points $\boldsymbol{r}$ below the line of tow, $\Lambda < 0$. It can be seen from figure 3(*a*) that below the line of tow only one system of waves exists, corresponding to values $\eta_\infty < \eta < \eta_r$. These are referred to as *lower flared* waves and are bounded below both the line of tow and the plane $r_{1z} = 0$ by the wave front defined by ϑ_r. The corresponding *upper flared* waves are bounded above the line of tow and below the plane $r_{1z} = 0$ and are given by $-\pi/2 < \eta < \eta_r$ in figure 3(*b*). Figure 3(*b*) also shows that for $\Lambda > 0$ and $\vartheta_c \leqslant \vartheta \leqslant \pi$, not only are upper flared waves present, but two more sets of waves also exist downstream of the point source. These are the *lower cusped* waves corresponding to $\eta_\infty < \eta < \eta_c$ and the *upper cusped* waves corresponding to $\eta_c < \eta < \pi/2$.

Figure 4(*a*) shows how the four values of η vary with Λ. In the limiting case as $\Lambda \to \pm\infty$, i.e. horizontal towing, $\eta_r \to \mp\pi/2$, $\eta_\infty \to 0$, $\eta_0 \to \mp\pi/2$ and $\eta_c \to \pm\pi/2$. In the other limiting case, vertical towing, as $\Lambda \to 0^+$, $\eta_r \to 0$, $\eta_\infty \to \pi/2$ and $\eta_c \to \pi/2$. As $\Lambda \to 0^-$, $\eta_r \to 0$, $\eta_\infty \to -\pi/2$ and $\eta_0 \to 0$. Figure 4(*b*) shows how the corresponding values of ϑ vary with Λ. Again in the limiting horizontal case, as $\Lambda \to \pm\infty$, $\vartheta_r \to \pi/2 \pm \pi/2$, $\vartheta_\infty \to \pi$, $\vartheta_0 \to \pi/2$ and $\vartheta_c \to \pi/2$. In the limiting vertical case, as $\Lambda \to 0^+$, $\vartheta_r \to \pi/2$, $\vartheta_\infty \to \pi$ and $\vartheta_c \to \pi$ and as $\Lambda \to 0^-$, $\vartheta_r \to 0$, $\vartheta_\infty \to \pi$ and $\vartheta_0 \to \pi/2$. The physical implications of these limiting values are that in the limiting horizontal tow case, there are no upper waves and in the limiting vertical tow case, there are no cusped waves. Upstream waves occur in the region where $\Lambda < 0$ and $\eta_0 \leqslant \eta \leqslant \eta_r$. The only values of Λ where $\eta_0 = \eta_r$ are $\Lambda = 0$ and $\Lambda = -\infty$, so in both limiting horizontal and vertical towing cases, no upstream waves are present and furthermore these are the only possible tow angles where no upstream waves are present.

Figure 5 shows how the centreplane $y = 0$ is divided up by the four angles ϑ_0, ϑ_∞, ϑ_c and ϑ_r and how a line of constant phase fits into the different regions. The line

https://doi.org/10.1017/S0022112003006815 Published online by Cambridge University Press

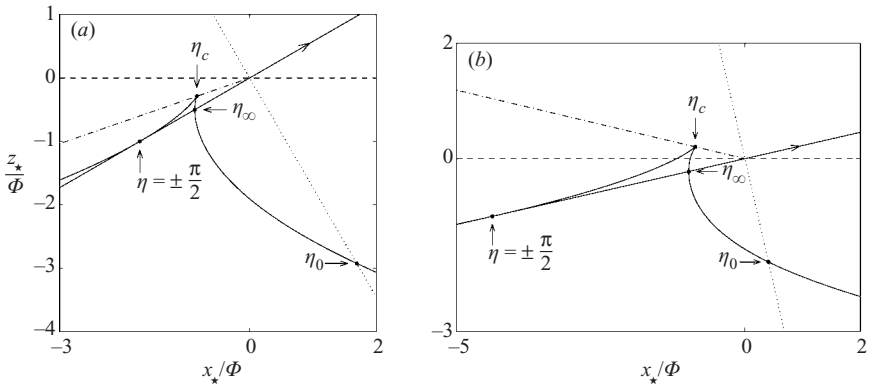


FIGURE 5. The tow line $\vartheta_\infty = \pi$ (solid), the line splitting the upstream and the downstream waves $\vartheta_0 = \pi/2$ (dotted), the horizontal plane through the source ϑ_r (dashed), the caustic ϑ_c (dash-dot): (*a*) angles $\alpha = \pi/3$ and (*b*) $\alpha = 3\pi/7$. To the left of $\eta = \pm\pi/2$ is the upper flared wave; between $\eta = \pm\pi/2$ and η_c is the upper cusped wave; between η_c and η_∞ is the lower cusped wave; to the right of η_∞ is the lower flared wave, intersecting the line ϑ_0 at η_0.

of constant phase touches the line of tow when $\eta = \pm\pi/2$, cuts the line of tow when $\eta = \eta_\infty$ and touches the caustic defined by $\vartheta = \vartheta_c$ when $\eta = \eta_c$. The line of constant phase cuts the line separating the downstream waves and the upstream waves when $\eta = \eta_0$.

As can be seen in figure 1 and equation (3.5), the angle ϑ is independent of the length of $\boldsymbol{r}_1$. Hence, from equation (3.7), η is also independent of the length of $\boldsymbol{r}_1$. This means that the direction of $\boldsymbol{R}(\tau_s)$ is only dependent on the direction of $\boldsymbol{r}_1$. Since the frequency ω, group velocity $\boldsymbol{c}_g$, and wavenumber $\boldsymbol{k}$ depend only on the direction of $\boldsymbol{R}$, it means that these quantities (ω, $\boldsymbol{k}$ and $\boldsymbol{c}_g$) are independent of the length of $\boldsymbol{r}_1$, and are hence radially invariant in the moving set of coordinates. It follows from this that, in a given direction, the boundary of the causality envelope due to the condition $\tau_s > 0$ is a distance $|\boldsymbol{c}_g - \boldsymbol{v}_0|t$ from the source (since $\boldsymbol{c}_{g1} = \boldsymbol{c}_g - \boldsymbol{v}_0$ is the group velocity in the moving reference frame). The distance from the position of the source to the causality envelope is given by

$$r_1 = |\boldsymbol{c}_{g1}|t = v_0 t \left\{ \frac{\cos^2\alpha}{(\cos\alpha \sin\eta + \cos\varpi \cos\eta)^2} + \cos^2\eta \right\}^{1/2}.$$

The dependence of the group velocity only on the direction of $\boldsymbol{r}_1$ also means that the causality envelope is self-similar with time. This wavefront is shown in figure 6 for the two cases $\alpha = \pi/3$ and $\alpha = 3\pi/7$ in the plane $y = 0$. The unmarked regions correspond to the regions with no waves present, i.e. the uniformly grey regions in figure 2. Region A_1 contains only upper flared waves. Region A_2 contains only lower flared waves. Region B contains both upper flared waves and upper cusped waves, but not lower cusped waves. This is because the lower cusped waves have propagated more slowly than the upper cusped waves. Region C contains upper flared waves, upper cusped waves and lower cusped waves. Regions in which more than one wave contributes to the superposition are henceforth referred to as 'regions of wave interference'. (These regions of interference were shown in two dimensions both theoretically and experimentally in Stevenson 1968.) Figure 7 shows the caustic wave front defined by $\vartheta = \vartheta_c$ and the wave front defined by $\vartheta = \vartheta_r$ for the two cases $\alpha = \pi/3$ and $\alpha = 3\pi/7$ (the remaining front given by the condition $\tau_s > 0$ is not

https://doi.org/10.1017/S0022112003006815 Published online by Cambridge University Press

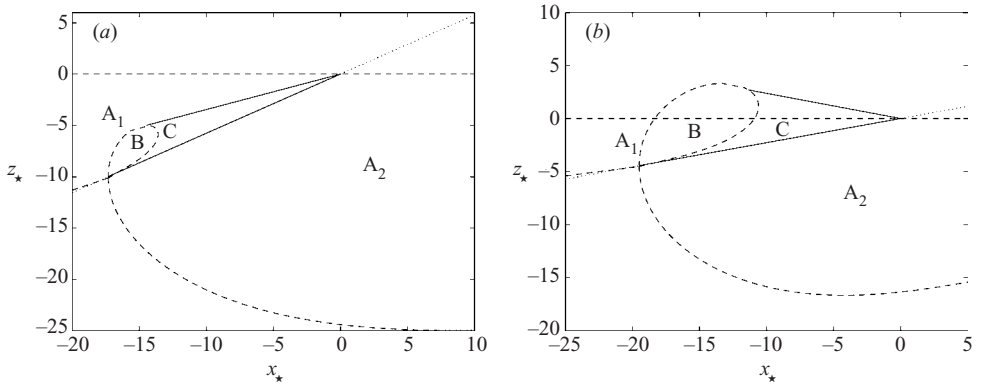


FIGURE 6. Wavefronts for (*a*) $\alpha = \pi/3$ and (*b*) $\alpha = 3\pi/7$ in the plane $y = 0$. The dotted line is the tow line. Region A_1 has only one wave contributing to the superposition, the upper flared waves. A_2 has only one wave contributing to the superposition, the lower flared waves. B has two waves contributing, upper flared waves and upper cusped waves. C has three waves contributing, upper flared waves, upper cusped waves and lower cusped waves.

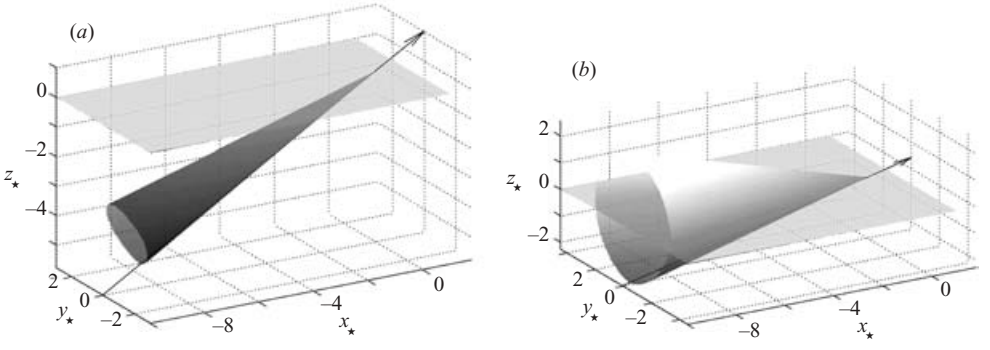


FIGURE 7. The wavefronts defined by $\vartheta = \vartheta_c$ and $\vartheta = \vartheta_r$ for (*a*) $\alpha = \pi/3$ and (*b*) $\alpha = 3\pi/7$.

shown). The regions outside the cones but below $z = 0$ correspond to regions A_1 and A_2 in figure 6.

The surfaces of constant phase for both the cusped waves and the flared waves are shown in figure 8.

3.3. *Non-oscillating spherical source*

In contrast to the point source case, when an extended source generates the wave field, there are two available length scales. There is a length scale from the size of the source (e.g. the radius of a sphere) and another length scale from the ratio of the tow velocity and the buoyancy frequency. The ratio of these two length scales is the Froude number; in the case of a sphere it is defined to be $Fr = v_0/Na$, where a is the radius of the sphere. Gorodtsov & Teodorovich (1980) showed that the energy lost to wave generation for a point source was infinite. However, in Gorodtsov & Teodorovich (1982) a form for an arbitrarily moving spherical source of radius a was given, namely

$$m(\boldsymbol{r}, t) = \frac{3}{2a} \{\boldsymbol{v}_0 \cdot \boldsymbol{r}(t)\} \, \delta(|\boldsymbol{r}(t)| - a), \tag{3.20}$$

https://doi.org/10.1017/S0022112003006815 Published online by Cambridge University Press

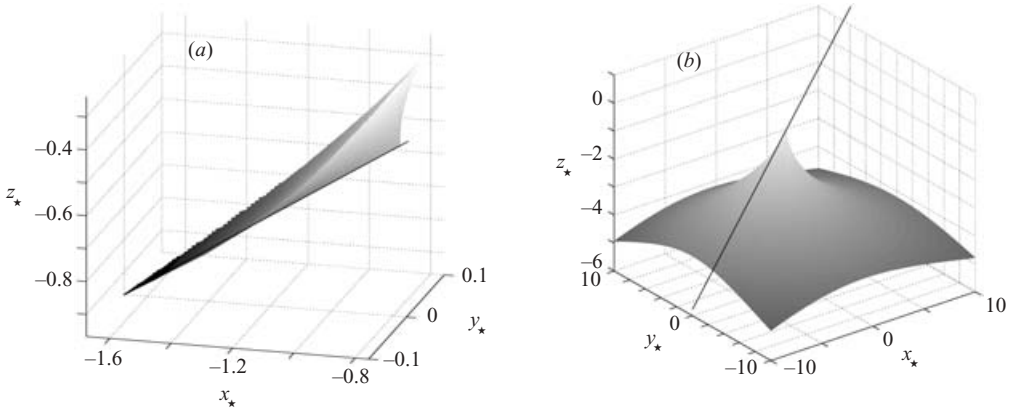


FIGURE 8. Surfaces of constant phase for (*a*) cusped waves and (*b*) flared waves for $\alpha = \pi/3$. The solid line is the line of tow.

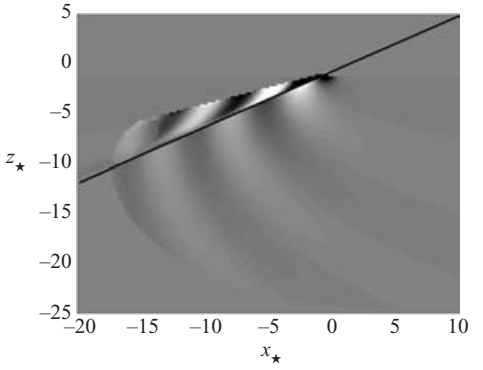


FIGURE 9. The vertical velocity field induced by towing a non-oscillating sphere for $t_\star = 20$. Here $Fr = 2$, $\alpha = \pi/3$ and $y_\star = 0$. This can be compared to figure 2 where the point source model was used.

and this was shown to give finite energy losses. The model in (3.20) will be used, replacing equation (2.3), to give the flow fields generated by a spherical source towed in an arbitrary direction. This was done for the horizontal case, $\alpha = \pi/2$ in Dupont & Voisin (1996).

The spatial Fourier transform of (3.20), for constant $\boldsymbol{v}_0$, is independent of time and is given by

$$M(\boldsymbol{k}, t) = \int_{\mathbb{R}^3} m(\boldsymbol{r}, t) \mathrm{e}^{\mathrm{i}\boldsymbol{k}\cdot\boldsymbol{r}} \, \mathrm{d}\boldsymbol{r} = 6\mathrm{i}\pi a^3 \, (\boldsymbol{v}_0 \cdot \boldsymbol{k}) \, \frac{j_1(ka)}{ka}, \tag{3.21}$$

where j_1 is a spherical Bessel function of the first kind, i.e.

$$j_1(x) = \frac{\sin x}{x^2} - \frac{\cos x}{x}. \tag{3.22}$$

Since $M(\boldsymbol{k}, t)$ is independent of t it shall be denoted $M(\boldsymbol{k})$.

The plots in figures 9 and 10 show the resulting vertical velocity field for a sphere with angle of tow $\alpha = \pi/3$, $Fr = 2$ and $t_\star = 20$. Figure 9 can be directly compared to figure 2; they both show the vertical velocity field for corresponding values of $t_\star$ and α, in the $y_\star = 0$ plane. The flow field in figure 9 shows the same interference region

https://doi.org/10.1017/S0022112003006815 Published online by Cambridge University Press

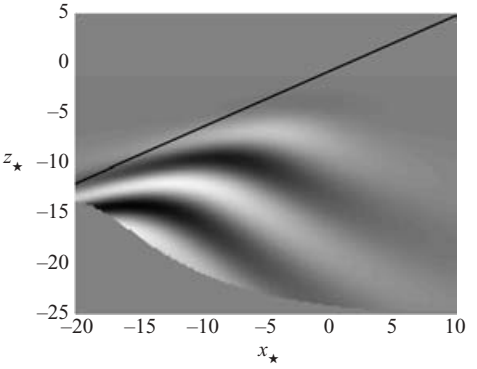


FIGURE 10. The vertical velocity field induced by towing a non-oscillating sphere for $t_\star = 20$. Here $Fr = 2$, $\alpha = \pi/3$ and $y_\star = 5$. Note that the plane $y_\star = 5$ does not intersect the wavefront cone, shown in figure 7 for the range of $x_\star$ and $z_\star$ shown and so only one wave is contributing to the field in this range. The colour scaling in this figure is, for illustration, ten times greater than in figures 9 and 11. The lower boundary of the waves is a wavefront defined by the causality envelope.

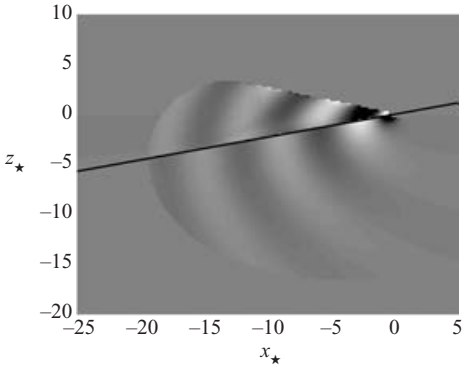


FIGURE 11. The vertical velocity field for a spherical source which has been towed at an angle $\alpha = 3\pi/7$, $Fr = 1$ for $t_\star = 20$. The axes have been non-dimensionalized as in figure 2. The dark black line is the tow line.

above the tow line that was present in figure 2. The plane $y_\star = 5$ shown in figure 10 does not intersect the conical region containing the cusped waves and so in the field shown, only one wave contributes to the superposition of the waves. Figure 11 shows the vertical velocity field generated by a sphere with angle of tow $\alpha = 3\pi/7$, $Fr = 1$ and $t_\star = 20$.

If non-parallel straight wave beams are emitted from a point they cannot cross in the flow region and hence cannot interfere with each other. This is not the case for extended, finite-sized (non-degenerate) sources since waves can be emitted from different parts of the source's surface. The factor $M(\boldsymbol{k}, \tau_s)$ in the expression for the internal potential (2.25) can be interpreted as interference due to the extended source, i.e. when $M(\boldsymbol{k}, \tau_s) = 0$ there is complete destructive interference. For a spherical source of the form (3.20) then waves with short wavelengths (i.e. large wavenumbers) undergo destructive interference. Comparison of figures 2 and 9 shows this to be the case as the amplitude of the waves in regions B and C for the point source is greater than that for the spherical source, but the amplitude of the waves in regions

https://doi.org/10.1017/S0022112003006815 Published online by Cambridge University Press

A_1 and A_2 is approximately the same. Also, for the specific source model in (3.20), waves with wavenumber k, where k satisfies $j_1(ka) = 0$, undergo complete destructive interference. This gives rise to interference patterns not observed in point source models.

4. Drag induced on sphere

In this section the wave drag induced on a sphere by the wave field is considered for general tow angle $0 \leqslant \alpha \leqslant \pi/2$, and general Froude number. This drag does not include the friction (viscous) drag, the inertial (form) drag (Batchelor 1967, § 5.11) or the buoyancy drag due to permanent deformation of the isopycnals as the sphere is towed, but will henceforth be referred to as the 'wave drag'.

When an object is towed through a stratified fluid, there is a deformation of the isopycnals. It has been shown (Hanazaki & Torres 2000; Torres, Ochoa & Castillo 2000) that a jet is consequently formed when the ispoycnals return to their original position. This results in an extra 'buoyancy' drag on the sphere (measured experimentally for a grid towed vertically with small Froude number in Higginson, Dalziel & Linden 2002) which is not due to the formation of internal waves and has therefore been neglected here.

The wave drag, D, is given for the three-dimensional case in Gorodtsov & Teodorovich (1982) as

$$D = \frac{\rho_0}{8\pi^2 v_0} \int_{-N}^{N} \int_{\mathbb{R}^3} |\omega|(N^2 - \omega^2)|M(\boldsymbol{k})|^2 \delta\left(\omega^2 \boldsymbol{k}^2 - N^2 \boldsymbol{k}_h^2\right) \delta\left(\omega - \boldsymbol{k} \cdot \boldsymbol{v}_0\right) \mathrm{d}\boldsymbol{k}\, \mathrm{d}\omega, \quad (4.1)$$

where $\boldsymbol{k}_h = \left(k_x, k_y, 0\right)$. This comes from a spectral form of the energy losses, due to internal wave generation, given in Gorodtsov & Teodorovich (1980).

Calculating the spectral form of the expression for the drag (4.1) avoids a number of problems associated with calculating the wave drag directly from the velocity or pressure fields as given in § 2 and § 3, which are far-field approximations. The drag calculation based on the pressure and velocity fields assumes that the source has moved along an infinite path, and so no closed domain can be found, through which to calculate the momentum flux, which is everywhere infinitely far from the source path.

For the case of steady tow in a horizontal direction, the expression for the wave drag D in (4.1) reduces to (Gorodtsov & Teodorovich 1982)

$$D = \rho_0 \left(\frac{3\pi a^2 N}{4}\right)^2 Fr \int_1^{\infty} \frac{J_{3/2}^2(\xi/Fr)}{\xi^3 \sqrt{\xi^2 - 1}}\, \mathrm{d}\xi\,; \quad (4.2)$$

this follows from (4.1) using the source (3.20), with spectrum (3.21). Greenslade (2000), compared (4.2) to the experimental data of Lofquist & Purtell (1984), and showed good agreement for $Fr \gtrsim 1$. The agreement is less good for $Fr \lesssim 1$, because for small Froude number the tow velocity and the wave speeds become comparable and nonlinear effects become significant, invalidating the linear theory (cf. § 2). Also, the source model (3.20) proposed by Gorodtsov & Teodorovich (1982) is only strictly valid for a vanishingly small stratification.

The general case can be calculated by first defining the vector $\boldsymbol{k}^\star$ as a rotation of the wavenumber vector $\boldsymbol{k}$. This is chosen so that $k_x^\star = \boldsymbol{k} \cdot \hat{\boldsymbol{r}}_0$ and $k_y^\star = k_y$ (a more

https://doi.org/10.1017/S0022112003006815 Published online by Cambridge University Press

detailed account is given in Appendix B). It follows, from (4.1), that†

$$D = \frac{\rho_0}{8\pi^2 v_0}\left\{\int_0^{N\cos\alpha}\int_{h_-(\omega)}^{h_+(\omega)} g(\xi,\omega)\,\mathrm{d}\xi\,\mathrm{d}\omega + \int_{N\cos\alpha}^{N}\left[\int_{-\infty}^{h_+(\omega)} g(\xi,\omega)\,\mathrm{d}\xi + \int_{h_-(\omega)}^{\infty} g(\xi,\omega)\,\mathrm{d}\xi\right]\mathrm{d}\omega\right\}, \quad (4.3)$$

where

$$h_\pm = \frac{\omega(\sqrt{N^2-\omega^2}\cos\alpha \pm \omega\sin\alpha)}{N^2\cos^2\alpha-\omega^2}, \quad (4.4)$$

and

$$g(\xi,\omega) = \frac{2\omega|M(\boldsymbol{k}^\star)|^2}{v_0}\sqrt{\frac{N^2-\omega^2}{(N^2\cos^2\alpha-\omega^2)(\xi-h_-)(h_+-\xi)}}. \quad (4.5)$$

The spectral source $M(\boldsymbol{k}^\star)$ is evaluated from

$$\left.\begin{aligned} k_x^\star &= \omega,\\ k_y^\star &= \left\{\frac{\omega^4}{v_0^2(N^2\cos^2\alpha-\omega^2)} - \frac{(N^2\cos^2\alpha-\omega^2)}{N^2-\omega^2}\left[k_z^\star - \frac{\omega N^2\sin\alpha\cos\alpha}{v_0(N^2\cos^2\alpha-\omega^2)}\right]^2\right\}^{1/2},\\ k_z^\star &= \frac{\xi\sqrt{N^2-\omega^2}-\omega\cos\alpha}{v_0\sin\alpha}. \end{aligned}\right\} \quad (4.6)$$

If $M(\boldsymbol{k})|_{\boldsymbol{k}\cdot\boldsymbol{v}_0=\omega}$ depends only on the modulus of $\boldsymbol{k}$, as in (3.21), then this can be greatly simplified since $ka = k^\star a = \xi/Fr$ in the first and third double integrals of equation (4.3), and $ka = k^\star a = -\xi/Fr$ in the second. Although g is singular at $\xi = h_\pm(\omega)$, they are integrable singularities and so each inner integral converges for a given value of ω, provided M is finite.

In the horizontal case $\alpha = \pi/2$, equation (4.3) simply reduces to (4.2) since the first double integral in (4.3) is identically zero, and the second integral becomes separable in ξ and ω. In the general case it is difficult to proceed analytically; however the above form is well suited to numerical evaluation.

As can be observed from equation (4.3), the expression for the wave drag falls naturally into two integrals: the first for $0 \leqslant \omega < N\cos\alpha$, and the second for $N\cos\alpha < \omega \leqslant N$. By considering the dispersion relation for internal waves (cf. § 2), it is clear that the integral over $N\cos\alpha < \omega \leqslant N$ corresponds to the drag due to waves in a double cone, vertex O_1 and semi-angle α.

It is usual to express the drag induced by the flow in terms of a *drag coefficient* (Batchelor 1967, § 5.11; Lofquist & Purtell 1984; Greenslade 2000) due to the waves, C_D, where $C_D = 2D/(\rho_0 v_0^2 \pi a^2)$. The plot in figure 12 shows the change in this drag coefficient for $Fr = 1$ as the tow angle varies. The curve is not symmetric about $\alpha = \pi/4$, initially decreasing from its value at $\alpha = 0$ until it reaches a minimum value at $\alpha \approx 2\pi/7$. The drag coefficient then increases again until it reaches its value at $\alpha = \pi/2$.

Typical parameter values for a thermal rising in the atmosphere (Warren 1960) are $a = 10\,\mathrm{m}$, $v_0 = 1\,\mathrm{m\,s^{-1}}$, $N = 0.01\,\mathrm{s^{-1}}$ and the kinematic viscosity $\nu = 10^{-5}\,\mathrm{m^2\,s^{-1}}$ giving $Re = 2\times10^6$ and $Fr = 10$. Experimental studies (Batchelor 1967, § 5.11) suggest

† It was pointed out to the authors during the refereeing process that this result was derived in a different, but equivalent, form in Gorodtsov, Reznik & Stepanyants (1997).

https://doi.org/10.1017/S0022112003006815 Published online by Cambridge University Press

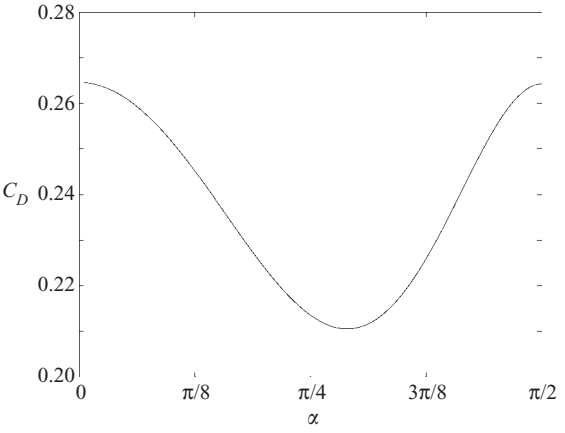


FIGURE 12. The wave drag coefficient C_D against angle to the vertical α, for $Fr = 1$.

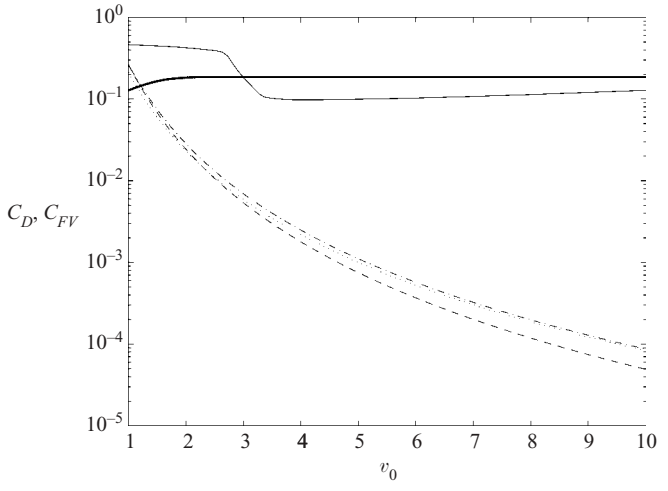


FIGURE 13. The magnitude of the combined form and viscous drag coefficient, C_{FV}, for a sphere as the Reynolds number is increased from 10^5 to 10^6 (thin solid) and as the Reynolds number is increased from 10^6 to 10^7 (thick solid); and the wave drag coefficient for a sphere as the Froude number increases from 1 to 10 being towed at: $\alpha = 0$ (dashed), $\alpha = \pi/4$ (dotted) and $\alpha = \pi/2$ (dashed-dotted).

a drag coefficient for a sphere towed in a homogeneous fluid at $Re = 2 \times 10^6$ of order $C_{FV} \sim O(0.2)$ and the present study suggests a value for the wave drag coefficient for a sphere at $Fr = 10$ of order $C_D \sim O(10^{-4})$. These typical values indicate that for a rising thermal the wave drag is of order 0.5% of the combined form and viscous drag, C_{FV}, as was found by Warren (1960). Hence, in the case of a typical rising thermal in the atmosphere, the wave drag is negligible.

Figure 13 shows a comparison between the relative orders of magnitude of the combined form and viscous drag, C_{FV}, and wave drag, C_D, for a sphere. For illustration, a sphere of radius 0.5 m has been chosen. The kinematic viscosity of air has been taken as $10^{-5}\,\mathrm{m^2\,s^{-1}}$ and the kinematic viscosity of water has been taken as $10^{-6}\,\mathrm{m^2\,s^{-1}}$. Hence as the speed of tow increases from $v_0 = 1\,\mathrm{m\,s^{-1}}$ to $v_0 = 10\,\mathrm{m\,s^{-1}}$, the Reynolds number (defined as $Re = 2v_0a/\nu$) for the sphere in air increases from

https://doi.org/10.1017/S0022112003006815 Published online by Cambridge University Press

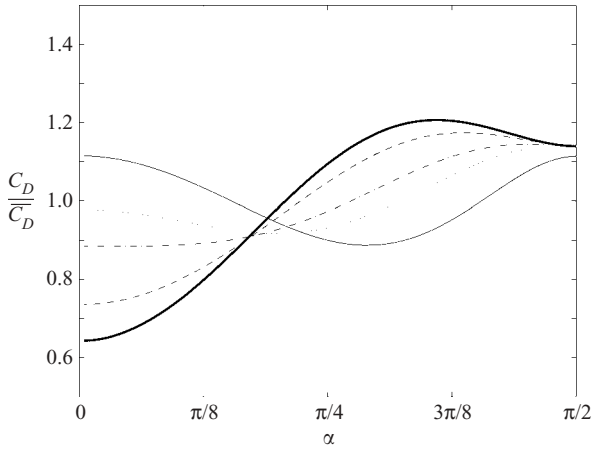


FIGURE 14. The scaled drag coefficient C_D against angle to the vertical α, for $Fr = 1$ (thin solid), $Fr = 2$ (dotted), $Fr = 3$ (dashed-dot), $Fr = 6$ (dashed), $Fr = 10$ (thick solid). The drag coefficient is scaled on the average drag, $\overline{C_D}$ for a given Froude number.

10^5 to 10^6 and the Reynolds number for the sphere in water increases from 10^6 to 10^7. The shown magnitudes of C_{FV} are empirical (Batchelor 1967, § 5.11). The thin solid line is C_{FV} for the sphere in air, the thick solid line is C_{FV} for the sphere in water. The buoyancy frequency has been taken to be $N = 2\,\mathrm{s}^{-1}$ and so as the speed increases from $v_0 = 1\,\mathrm{m\,s}^{-1}$ to $v_0 = 10\,\mathrm{m\,s}^{-1}$, the Froude number also increases from $Fr = 1$ to $Fr = 10$ (note that this is not a realistic figure for atmospheric or oceanic applications). The dashed line is C_D for the sphere towed at $\alpha = 0$ to the vertical, the dotted line is C_D for the sphere towed at $\alpha = \pi/4$ to the vertical and the dashed-dotted line is C_D for the sphere towed at $\alpha = \pi/2$ to the vertical. It can be seen that for $Fr \gtrsim 3$, the wave drag is significantly less than the form drag. (At $Fr = 3$, $C_{FV} \sim 20C_D$.) However, for $1 \lesssim Fr \lesssim 3$ and $Re \gtrsim O(10^5)$, the wave drag is not negligible. In fact even for a relatively low Reynolds number, $Re \sim O(10^3)$, and $Fr \approx 1$, the wave drag is as much as 50% of the form and viscous drag. Figure 13 also shows that for a given tow angle the wave drag decreases as the Froude number increases. This is because as the Froude number increases, the amplitude of the generated internal waves decreases and so the magnitude of the momentum flux away from the source decreases and hence there is less drag.

Figure 14, where the wave drag coefficient has been scaled on its average value, $\overline{C_D}$ (averaged over all angles $0 \leqslant \alpha \leqslant \pi/2$ for a given Froude number), shows that the tow angle which gives least wave drag coefficient is not a constant, but is dependent on the Froude number. It demonstrates how the angle of minimum wave drag decreases as the Froude number increases. As the Froude number increases, the wave drag coefficient decreases and the tow angle of minimum drag tends towards zero, i.e. vertical towing. It follows that the choice of tow angle can affect the magnitude of the drag coefficient, for $Fr = 1$, by a factor of up to approximately 20% and up to a factor of almost 47% for $Fr = 10$.

5. Conclusions

In § 3 it was shown that for the general case $0 \leqslant \alpha \leqslant 2\pi$, finding the vector $\boldsymbol{R}(\tau_s)$, which is the vector from the point where the internal wave was created at S to its point

https://doi.org/10.1017/S0022112003006815 Published online by Cambridge University Press

of reception at M (see figure 1), involved solving a cubic equation in $\tan\eta$ (3.7). This equation was of exactly the same form as in the vertical case, $\alpha = 0$ (3.3). This result showed that the flow field was built up of a number of regions. In the first region, no waves had or could propagate due to the causality condition, or the radiation condition. Other regions may have a single significant wave mode, containing only flared waves, or comprise a superposition of two waves (upper flared waves and upper cusped waves) or three waves (upper flared waves, upper cusped waves and lower cusped waves). The number of waves contributing to the superposition is given by the number of real roots of equation (3.7), and whether the corresponding waves satisfy the causality and radiation conditions. This means that wavefronts are not only found on the boundary of the disturbed and undisturbed fluid (where the waves have not yet propagated), but are also found inside the disturbed flow region. For both the point source and the extended source, where the flow has more than one wave contributing to the flow field at a point, the flow is given by the superposition of all the waves and exhibits wave interference. The finite, non-degenerate, size of the extended source means that waves with short wavelengths undergo significant cancellation; however, this destructive interference is not experienced by waves with long wavelengths. This interference is because non-parallel wave beams originating at the source can cross in the flow field, which cannot happen for a point source.

It should also be noted that when internal gravity waves are generated by a source which oscillates about a fixed point, there is a clear cut-off frequency, above which internal waves are not generated. This is when $\omega_0/N > 1$, where ω_0 is the oscillation frequency of the source. However, when internal waves are generated by a steadily translating source there is no analogous cut-off frequency. It is not the case that when $Fr > 1$ no internal are generated.

In § 4 the expression for the drag coefficient due to wave generation was calculated for general Froude number and tow angle. It shows that the magnitude of the wave drag depends on the tow angle and that, for all angles of tow, the drag coefficient decreases as the Froude number increases. It was also shown that for flows with Froude numbers such that $1 \lesssim Fr \lesssim 3$ and $Re \gtrsim O(10^3)$ the wave drag was not negligible compared to the form and viscous drags. The scaled drag coefficient plot (figure 14) shows that the angle which gives the minimum drag coefficient for a given Froude number is not constant, but decreases as the Froude number increases. It also shows that the angle of tow can affect the magnitude of the drag coefficient for a given Froude number by a significant amount. It can be seen from the figures in § 3 that the waves produced are not symmetric about the line of tow and hence a lift force acts on the sphere. The method used to determine the wave drag does not allow calculation of the lift; however an expression for this is given in Gorodtsov *et al.* (1997).

The authors wish to express their thanks to Dr Bruno Voisin for many helpful comments on the work presented here, Dr Rick Munro for his help with the many drafts and in particular an anonymous referee who suggested much of the analysis presented in § 3.2. This work was funded by studentship NER/S/A/2000/03262 from the Natural Environment Research Council.

Appendix A. Oscillating point source

In this Appendix a point source of purely oscillatory strength, i.e. with $\omega_0 \neq 0$ in equation (2.3), is considered. The method adopted in this section is different to that

https://doi.org/10.1017/S0022112003006815 Published online by Cambridge University Press

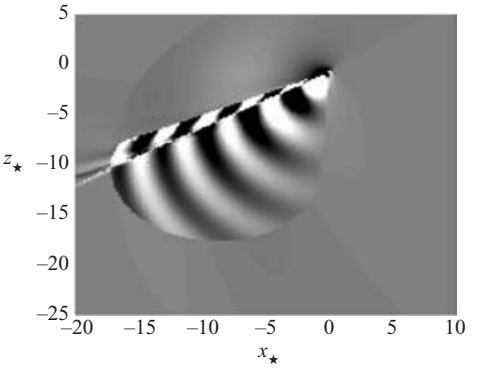


FIGURE 15. The vertical velocity field for an oscillating point source which has been towed at an angle $\alpha = \pi/3$ with $v_0 = 1$, $N = 1$ and $\Upsilon = 0.6$ for $t_\star = 20$. Here $y_\star = 0$, and so this can be directly compared to figures 2 and 9 where $\Upsilon = 0$.

used in Voisin (1994). Instead of defining quantities in terms of the Doppler frequency, ω/N, the analogous equation to (3.7) is found. It is a polynomial of order six, as is the equation obtained for the Doppler frequency. The expressions for the fluid velocity, $\boldsymbol{u}(\boldsymbol{r}, t)$, and pressure perturbation, $P(\boldsymbol{r}, t)$, are given in (2.16) and (2.17).

The modified version of equation (3.4) becomes

$$\left(\sin\eta - \frac{\cos\eta\cos\vartheta}{\sin\vartheta}\right)\left(\sin\eta - \frac{\cos\alpha}{\cos\varphi}\right) - 1 = \mp\frac{\Upsilon}{|\cos\varphi|}, \tag{A 1}$$

where Υ is the frequency ratio ω_0/N. Squaring equation (A 1) gives a sixth-order polynomial in $\tan\eta$, i.e.

$$\sum_{n=0}^{6} c_n \tan^n\eta = 0, \tag{A 2}$$

whose coefficients are

$$\left.\begin{aligned}
c_0 &= (\cos\varpi\sin\vartheta - \cos\vartheta\cos\alpha)^2 - \Upsilon^2\sin^2\vartheta,\\
c_1 &= 2\sin\vartheta\cos\vartheta(\cos\varpi^2 - 2\cos^2\alpha) + 2\cos\varpi(2\sin^2\vartheta - \cos^2\vartheta)\cos\alpha,\\
c_2 &= (\cos\varpi\cos\vartheta + 2\sin\vartheta\cos\alpha)^2 - 3\Upsilon^2\sin^2\vartheta,\\
c_3 &= 2\sin\vartheta\cos\alpha(\cos\varpi\sin\vartheta - \cos\vartheta\cos\alpha),\\
c_4 &= 2\cos\varpi\sin\vartheta\cos\vartheta\cos\alpha + (4\cos^2\alpha - 3\Upsilon^2)\sin^2\vartheta,\\
c_5 &= 0,\\
c_6 &= (\cos^2\alpha - \Upsilon^2)\sin^2\vartheta.
\end{aligned}\right\} \tag{A 3}$$

Note that equation (A 2) is exactly the square of (3.7) when $\Upsilon = 0$.

It follows that, for the oscillating point source, the solutions come in pairs and are called the *sum* and *difference* waves, corresponding to the choice of sign in equation (A 1). The expressions for the pressure and velocity are the sum over all $\boldsymbol{R}(\tau_{s\pm})$, which satisfy the causality and radiation conditions.

Figure 15 shows the vertical component of the velocity field in the $(x_\star, 0, z_\star)$-plane, for an oscillating point source having been towed for $t_\star = 20$. The angle of tow is $\alpha = \pi/3$, the Froude number is $Fr = 2$ and the frequency ratio is $\Upsilon = 0.6$. Taking the limit as $\omega_0 \to 0$ recovers the solution for $\omega_0 = 0$. This happens because (A 2) becomes the square of (3.7), hence the repeated roots are both the sum and difference solutions,

https://doi.org/10.1017/S0022112003006815 Published online by Cambridge University Press

thus making them identical. The expressions for the pressure and velocity (2.16), (2.17) are therefore complex conjugates whose sum gives (2.12) and (2.13).

The number of wavefronts within the flow field is increased, since twice as many waves, with different speeds of propagation, contribute to the flow field, as in the non-oscillatory case. A more detailed analysis of the waves (as in § 3.2) has not been attempted.

Appendix B. Details of drag calculation

Equation (4.3) was derived from (4.1) by first defining the rotated wavenumber vector $\boldsymbol{k}^\star = (k_x^\star, k_y^\star, k_z^\star)$ as

$$\boldsymbol{k}^\star = (k_x \sin\alpha + k_z \cos\alpha,\, k_y,\, -k_x \cos\alpha + k_z \sin\alpha). \tag{B 1}$$

It follows that $\delta(\omega - \boldsymbol{k}\cdot\boldsymbol{v}_0) = \delta(k_x^\star - \omega/v_0)/v_0$, so the first integration is performed over $k_x^\star$ and, within the integrand of (4.1), $k_x^\star = \omega/v_0$. Hence

$$\delta(\omega^2|\boldsymbol{k}|^2 - N^2|\boldsymbol{k}_h|^2) = \frac{1}{N^2-\omega^2}\,\delta\left(k_y^{\star 2} - \left[\frac{\omega^4}{v_0^2(N^2\cos^2\alpha-\omega^2)} - \frac{N^2\cos^2\alpha-\omega^2}{N^2-\omega^2}\left\{k_z^\star - \frac{\omega N^2 \sin\alpha\cos\alpha}{v_0(N^2\cos^2\alpha-\omega^2)}\right\}^2\right]\right).$$

Provided $M(k_y^\star) = M(-k_y^\star)$ then

$$\delta(\omega^2|\boldsymbol{k}|^2 - N^2|\boldsymbol{k}_h|^2) = \frac{2}{N^2-\omega^2}\left[\frac{\omega^4}{v_0^2(N^2\cos^2\alpha-\omega^2)} - \frac{(N^2\cos^2\alpha-\omega^2)}{N^2-\omega^2} \times \left\{k_z^\star - \frac{\omega N^2\sin\alpha\cos\alpha}{v_0(N^2\cos^2\alpha-\omega^2)}\right\}^2\right]^{-1/2} \delta\left(k_y^\star - \left[\frac{\omega^4}{v_0^2(N^2\cos^2\alpha-\omega^2)} - \frac{(N^2\cos^2\alpha-\omega^2)}{N^2-\omega^2}\left\{k_z^\star - \frac{\omega N^2\sin\alpha\cos\alpha}{v_0(N^2\cos^2\alpha-\omega^2)}\right\}^2\right]^{1/2}\right). \tag{B 2}$$

and the integral is taken for $0 \leqslant k_y^\star < \infty$. This means that within the integrand

$$k_y^{\star 2} = \frac{\omega^4}{v_0^2(N^2\cos^2\alpha-\omega^2)} - \frac{(N^2\cos^2\alpha-\omega^2)}{N^2-\omega^2}\left\{k_z^\star - \frac{\omega N^2\sin\alpha\cos\alpha}{v_0(N^2\cos^2\alpha-\omega^2)}\right\}^2. \tag{B 3}$$

The conditions on $k_y^\star$ being real are used to set the limits of integration for $k_z^\star$. Explicitly, for $0 \leqslant \omega < N\cos\alpha$,

$$\frac{\omega}{v_0}\frac{N^2\sin\alpha\cos\alpha - \omega\sqrt{N^2-\omega^2}}{N^2\cos^2\alpha-\omega^2} \leqslant k_z^\star \leqslant \frac{\omega}{v_0}\frac{N^2\sin\alpha\cos\alpha + \omega\sqrt{N^2-\omega^2}}{N^2\cos^2\alpha-\omega^2}, \tag{B 4}$$

and for $N\cos\alpha < \omega \leqslant N$,

$$\left.\begin{aligned} k_z^\star &\geqslant \frac{\omega}{v_0}\frac{\omega\sqrt{N^2-\omega^2} - N^2\sin\alpha\cos\alpha}{\omega^2 - N^2\cos^2\alpha}, \\ \text{or} \qquad k_z^\star &\leqslant \frac{\omega}{v_0}\frac{-\omega\sqrt{N^2-\omega^2} - N^2\sin\alpha\cos\alpha}{\omega^2 - N^2\cos^2\alpha}. \end{aligned}\right\} \tag{B 5}$$

https://doi.org/10.1017/S0022112003006815 Published online by Cambridge University Press

This condition forces the integral in (4.3) to be split over the two separate ranges for ω. The substitution

$$k_z^\star = \frac{\xi\sqrt{N^2-\omega^2}-\omega\cos\alpha}{v_0\sin\alpha}, \tag{B 6}$$

is made to make comparison with equation (4.2) straightforward. The limits on $k_z^\star$ are transformed to limits on ξ, and are given by $h_\pm$ as in equation (4.4). Once the Jacobians for all the transformations have been taken into account, the integrand $g(\xi,\omega)$ of equation (4.5) is found.

REFERENCES

Batchelor, G. K. 1967 *An Introduction to Fluid Dynamics*. Cambridge University Press (Cambridge Mathematical Library Edition 2000).

Dupont, P. 1995 Ondes internes engendrées par une source oscillante en mouvement. PhD thesis, L'Université Joseph Fourier, Grenoble.

Dupont, P. & Voisin, B. 1996 Internal waves generated by a translating and oscillating sphere. *Dyn. Atmos. Oceans* **23**, 289–298.

Gorodtsov, V. A., Reznik, S. N. & Stepanyants, Y. A. 1997 Radiative forces acting on point sources moving in a stratified fluid. *J. Exp. Theor. Phys.* **85**, 276–284. (Translation from *Zh. Éksp. Teor. Fiz.* **112**, 507–523.)

Gorodtsov, V. A. & Teodorovich, E. V. 1980 On the generation of internal waves in the presence of uniform straight-line motion of local and nonlocal sources. *Izv. Atmos. Ocean. Phys.* **16**, 9 699–704. (Translation from *Izv. Akad. Nauk SSSR Fiz. Atmos. Okeana* **16**, 954–961.)

Gorodtsov, V. A. & Teodorovich, E. V. 1982 Study of internal waves in the case of rapid horizontal motion of cylinders and spheres. *Fluid Dyn.* **17** (6), 893–898 1983. (Translation from *Izv. Akad. Nauk SSSR, Mekh. Zhid. i Gaza* **17** (6), 94–100.)

Greenslade, M. D. 2000 Drag on a sphere moving horizontally in a stratified fluid. *J. Fluid Mech.* **418**, 339–350.

Hanazaki, H. & Torres, C. R. 2000 Jet and internal waves generated by a descending sphere in a stratified fluid. In *Proc. 5th Intl Symposium on Stratified Flows* (ed. G. A. Lawrence, R. Pieters, & N. Yonemitsu).

Hart, R. W. 1981 Generalised scalar potentials for linearized three-dimensional flows with vorticity. *Phys. Fluids* **24**, 1418–1420.

Higginson, R. C., Dalziel, S. B. & Linden, P. F. 2002 The drag on a vertically moving grid of bars in a linearly stratified fluid. *Exps. Fluids* (submitted).

Lighthill, M. J. 1960 Studies on magneto-hydrodynamics waves and other anisotropic wave motions. *Phil. Trans. R. Soc. Lond.* A **252**, 397–430.

Lighthill, M. J. 1965 Group velocity. *J. Inst. Maths Applics.* **1**, 1–28.

Lighthill, M. J. 1967 On waves generated in dispersive systems by travelling forcing effects, with applications to the dynamics of rotating fluids. *J. Fluid Mech.* **27**, 725–752.

Lighthill, M. J. 1978 *Waves in Fluids*. Cambridge University Press.

Lofquist, K. E. B. & Purtell, L. P. 1984 Drag on a sphere moving horizontally through a stratified liquid. *J. Fluid Mech.* **148**, 271–284.

MacKinnon, R. F., Mulley, R. & Warren, F. W. G. 1969 Some calculations of gravity wave resistance in an inviscid stratified fluid. *J. Fluid Mech.* **38**, 61–73.

Miles, J. W. 1971 Internal waves generated by a horizontally moving source. *Geophys. Fluid Dyn.* **2**, 63–87.

Peat, K. S. & Stevenson, T. N. 1975 Internal waves around a body moving in a compressible density-stratified fluid. *J. Fluid Mech.* **70**, 673–688.

Rarity, B. S. H. 1967 The two-dimensional wave pattern produced by a disturbance moving in an arbitrary direction in a density stratified liquid. *J. Fluid Mech.* **30**, 329–336.

Rehm, R. G. & Radt, H. S. 1975 Internal waves generated by a translating oscillating body. *J. Fluid Mech.* **68**, 235–258.

Reitz, J. R. & Milford, F. J. 1960 *Foundations of Electromagnetic Theory*. Addison-Wesley.

https://doi.org/10.1017/S0022112003006815 Published online by Cambridge University Press

Smirnov, S. A. & Chashechkin, Yu. D. 1998 Internal lee (joined) waves at an arbitrary orientation of the incident flow. *Izv. Atmos. Ocean Phys.* **34**, 475–482. (Translation from *Izv. Akad. Nauk Fiz. Atmos. Okeana* **34**, 528–536.)

Stevenson, T. N. 1968 Some two-dimensional internal waves in a stratified fluid. *J. Fluid Mech.* **33**, 715–720.

Stevenson, T. N. & Thomas, N. H. 1969 Two-dimensional internal waves generated by a travelling oscillating cylinder. *J. Fluid Mech.* **36**, 505–511.

Torres, C. R., Ochoa, J. & Castillo, J. 2000 Numerical experiments of stratified flow past an impulsively started sphere. In *5th Intl Symp. on Stratified Flows* (ed. G. A. Lawrence, R. Pieters & N. Yonemitsu).

Voisin, B. 1991 Internal wave generation in uniformly stratified fluids. Part 1. Green's function and point sources. *J. Fluid Mech.* **231**, 439–480.

Voisin, B. 1994 Internal wave generation in uniformly stratified fluids. Part 2. Moving point sources. *J. Fluid Mech.* **261**, 333–374.

Warren, F. W. G. 1960 Wave resistance to vertical motion in a stratified fluid. *J. Fluid Mech.* **7**, 209–229.

https://doi.org/10.1017/S0022112003006815 Published online by Cambridge University Press